VARIATIONAL DATA ASSIMILATION IN THE TROPICS USING PRECIPITATION DATA

T Tsuyuki
Japan Meteorological Agency
Tokyo, Japan

Summary: This paper investigates the feasibility of four-dimensional variational data assimilation (4D-VAR) in the tropics using precipitation data. Assimilation experiments using simulated observations and real observations are carried out with a global primitive equation model including smoothed moist processes. Positive impacts of including moist processes in the adjoint model is demonstrated. It is shown that appropriate control of gravity wave level is important for faster convergence of 4D-VAR with moist processes included.

1. INTRODUCTION

Numerical weather prediction (NWP) in the tropics is more difficult than in the Northern Hemisphere extratropics. One reason for this is the relative lack of conventional observations. Another reason is the lack of a simple dynamical relationship between the mass and wind fields. This makes it difficult to design an appropriate multivariate statistical covariance model. A scale analysis of synoptic-scale circulations in the tropics shows that the primitive equations must be applied to analyze tropical precipitating disturbances (Holton, 1992). Four-dimensional variational data assimilation (4D-VAR) imposes no limitation on the type of data to be assimilated. In particular, it is appropriate for assimilating asynoptic satellite data. Such data are indispensable in producing a good tropical analysis. Furthermore, 4D-VAR is a comprehensive multivariate analysis using model dynamics. Thus, benefits from 4D-VAR may be greater in the tropics than in the extratropics. Although the performance of 4D-VAR has been examined by several authors with global NWP models (e.g., Thépaut and Courtier, 1991; Navon et al., 1992; Thépaut et al., 1993a, 1993b; Zou et al., 1993) and midlatitude regional NWP models (e.g., M. Zupanski, 1993; Zupanski and Mesinger, 1995), application of 4D-VAR in the tropics has not yet been fully examined.

The success of physical initialization proposed by Krishnamurti et al. (1984) provides promise for assimilating precipitation data for a better tropical analysis. 4D-VAR is capable of assimilating precipitation data in a straightforward way, provided that the assimilation model (forward model) and the corresponding adjoint model include a treatment of moist processes. The major advantages of 4D-VAR over physical initialization are (1) 4D-VAR uses the full model dynamics to adjust the model variables to the observed precipitation, (2) precipitation data errors can be correctly handled, and (3) 4D-VAR does not require synthesizing precipitation data from other observations.

In contrast to the extratropical atmosphere, cumulus convection plays a dominant role in determining large-scale atmospheric flow in the tropics. This property makes it essential to include parameterization of cumulus convection in 4D-VAR for tropical data assimilation. Inclusion of physical parameterizations, however, introduces a difficulty to 4D-VAR procedures. Since the physics are far more nonlinear than the dynamics, the tangent-linear approximation is less valid for a model with physics than for the same model without physics. In particular, threshold processes in parameterization schemes make a cost function discontinuous

or nondifferentiable. These strong nonlinearities degrade the efficiency of commonly used minimization algorithms. This is one of the problems to solve for applying 4D-VAR to tropical data assimilation.

This paper reports on the author's recent study on the feasibility of 4D-VAR in the tropics using precipitation data (Tsuyuki, 1996a, 1996b, 1996c). Two data assimilation experiments are carried out using a global primitive equation model with smoothed moist processes. In the first experiment, truth is provided by the full-physics model and observations are prepared by adding random error to the truth. The assimilation model and the adjoint model include moist processes, horizontal diffusion, and simplified surface friction only. In the second experiment, real observations are assimilated using the full-physics assimilation model and the reduced-physics adjoint model. Assimilated data are radiosonde and pibal data over globe and Special Sensor Microwave Imager (SSM/I) precipitation rates over the tropical oceans. Positive impacts of including the moist processes in the adjoint model is demonstrated. Emphasis is placed on the importance of appropriate control of gravity wave level for faster convergence of 4D-VAR with moist processes included.

This manuscript is organized as follows. A description of the model with the smoothed moist processes is presented in Section 2. Results from a column model assimilation experiment are also discussed in this section to show positive impacts of smoothing the moist processes. The experimental design and results of the first and the second experiments are described in Section 3 and Section 4, respectively. Conclusions are summarized in Section 5.

2. MODEL DESCRIPTION

The model is a low-resolution version of the Florida State University global spectral model (FSU-GSM). It has a horizontal resolution of triangular truncation at total wavenumber 42 with 12 levels in the vertical (T42L12). The number of Gaussian grid points is 64 (latitude) × 128 (longitude). The vertical coordinate is sigma, defined as

$$\sigma = \frac{p}{p_s}, \tag{1}$$

where p is the pressure, and p_s is the surface pressure. The vertical levels where velocity is defined are σ = 0.1, 0.2, 0.3, 0.4, 0.5, 0.6, 0.7, 0.8, 0.85, 0.9, 0.95, 0.99. The model state variables are vorticity, divergence, virtual temperature, dewpoint depression, and the logarithm of surface pressure. The former three variables are defined at all model levels, while dewpoint depression is defined only at the lowest 10 levels. The time step is 1200 s. The physics include radiation (Chang, 1979), surface fluxes (Businger et al., 1971), planetary boundary layer, vertical diffusion (Louis, 1979), horizontal diffusion, dry convective adjustment, large-scale condensation and evaporation, and deep cumulus convection (Krishnamurti et al., 1983). The latter three physical processes are referred to as the moist processes in this paper. Note that dry convective adjustment is included as a moist process.

The assimilation model used in the first experiment and the adjoint model include moist processes, horizontal diffusion, and simplified surface friction only. This package of physics is hereafter referred to as reduced physics. For the simplified surface friction a simple scheme for surface drag is taken from Thépaut et al.

(1993b). The following friction term is added to the momentum equation at the lowest two model levels:

$$F_{\mathrm{PBL}} = -\frac{u_*}{h}\frac{k}{\ln\left(\frac{z_K}{z_0}\right)} v_K , \tag{2}$$

where u_* is the surface friction velocity, h is the thickness of the planetary boundary layer, k is von Kalman's constant, z_0 is the roughness length, z_K is the height of the lowest model level, and v_K is the velocity at this level.

D. Zupanski (1993) demonstrated that discontinuities in a cumulus parameterization scheme had adverse effects on 4D-VAR. She modified the scheme to render it more continuous for variational data assimilation. In view of her results, several types of discontinuity in the original parameterization schemes of the moist processes are removed in this study. A modified Kuo scheme is used for parametrizing deep cumulus convection in the FSU-GSM. This scheme has several discontinuities that make the cost function discontinuous. First, the cloud base height is defined as the lowest model level satisfying the following four conditions: conditionally unstable stratification, upward velocity, upward moisture advection, and the condition that relative humidity exceeds a threshold value. It is easily seen that these specifications introduce discontinuous changes in cloud base height. The smoothed scheme defines the cloud base height as the lowest conditionally unstable level above the lifting condensational level, so that it is easy to remove discontinuities. Second, the cloud base and cloud top are assigned to one of the model levels as in most of the other atmospheric models. In the smoothed scheme, the cloud base and cloud top heights are allowed to assume any values. Thus, most of the discontinuous changes in cloud thickness are avoided except for a discontinuous change in cloud top height associated with the existence of an inversion layer. Third, a step function condition involving cloud thickness and relative humidity at cloud base is used to invoke deep cumulus convection. This is replaced by a smooth threshold function in the smoothed scheme. A similar smooth threshold function is also applied to remove a discontinuity from the large-scale condensation and evaporation algorithm. A few other types of discontinuity in the Kuo scheme are left unchanged for the sake of simplicity.

The removal of discontinuities, however, sometimes introduces locally large gradients in the cost function around discontinuous points. Although mathematically the gradient of the cost function is not defined at a discontinuous point, the adjoint method yields a finite gradient even at a discontinuous point. Fitting a smoothing function over the discontinuity makes the cost function continuous and differentiable, but the magnitude of the gradient of the smoothed cost function around the discontinuous point is likely to be much larger than that of the gradient of the discontinuous cost function calculated by the adjoint method. Care should be exercised over this point when removing discontinuities from physical parameterization schemes. Since physical processes are highly nonlinear, it may be inevitable that the cost function has a locally large gradient. It is desirable to avoid encountering such a locally large gradient during the minimization process because it may considerably degrade convergence performance.

Positive impacts of the above smoothing are demonstrated by a column model assimilation experiment using simulated data. The governing equations of the column model are the same as those of the FSU-GSM, except that the prediction equations for vorticity and divergence are excluded and that the horizontal advection

terms are neglected. Truth is a simulation with the column model starting from a reference state with a prescribed wind field. The length of the assimilation window is set to 6 hours Observations for the model state variables without error are available at the beginning and end of the assimilation window. The initial guess is the reference state perturbed by normally distributed random error. The experiment consists of 20 cases using different perturbations to the reference state.

Figure 1 shows cost functions plotted as a function of the number of function calls for the original version and the smoothed version of moist processes. The cloud-base specifications used in the smoothed version is also used in the original version in this experiment. The cost function is plotted on a logarithmic scale. Note that the abscissa is not the number of iterations. One function call consists of one forward integration of the assimilation model and one backward integration of the adjoint model. One iteration of the unconstrained minimization algorithm sometimes requires more than one function call due to line search. It is seen that the minimization converges for all cases even for the original version, but convergence rates for the smoothed version are faster and less case dependent.

3. ASSIMILATION EXPERIMENT USING SIMULATED DATA

3.1 **Experimental design**

The first experiment assimilates simulated observations. Since a reliable estimate of precipitation in the global tropics is difficult, simulated data approach may be suitable as a first step. The truth is provided by a simulation run with the full-physics model starting from an initialized objective analysis at 12 UTC 27 July 1979 prepared by the European Centre for Medium-range Weather Forecasts (ECMWF). In order to avoid problems associated with model spinup, the simulated atmospheric state 48 hours after the initial condition is taken as the target analysis. This time is set to $t = 0$ h. The assimilation window is the 6-hour period from $t = -6$ h to $t = 0$ h, and the simulation from $t = -18$ h to $t = -12$ h is used as the initial guess. Since overly optimistic results may be obtained if the same model is used to both generate and assimilate the simulated data, the assimilation model and the adjoint model include the reduced physics. However, the final analysis is obtained by integrating the full-physics model from the initial condition at $t = -6$ h determined by the minimization.

The cost function consists of a discrepancy term between model and observations and a penalty term for suppressing gravity wave noise, and does not include a background term:

$$J(\boldsymbol{x}_0) = \frac{1}{2}[\boldsymbol{H}(\boldsymbol{x}) - \boldsymbol{y}]^{\mathrm{T}}\mathbf{O}^{-1}[\boldsymbol{H}(\boldsymbol{x}) - \boldsymbol{y}] + \frac{1}{2}r\left(\frac{\partial \boldsymbol{D}}{\partial t}\right)^{\mathrm{T}}\mathbf{W}\frac{\partial \boldsymbol{D}}{\partial t}. \tag{3}$$

In the first term on the right-hand side, $\boldsymbol{x}$ denotes the model state variables at all time levels in the assimilation window, $\boldsymbol{y}$ the observations available in the assimilation window, $\boldsymbol{H}$ the observation operator that converts the model state variables to observed variables and interpolates from model grid points to observation points, $\mathbf{O}$ the observation error covariance matrix. The second term is the penalty term which controls the magnitude of the global mean of the divergence time tendency. This term helps to restrict possible solutions when the minimization problem is underdetermined due to insufficient observational data.

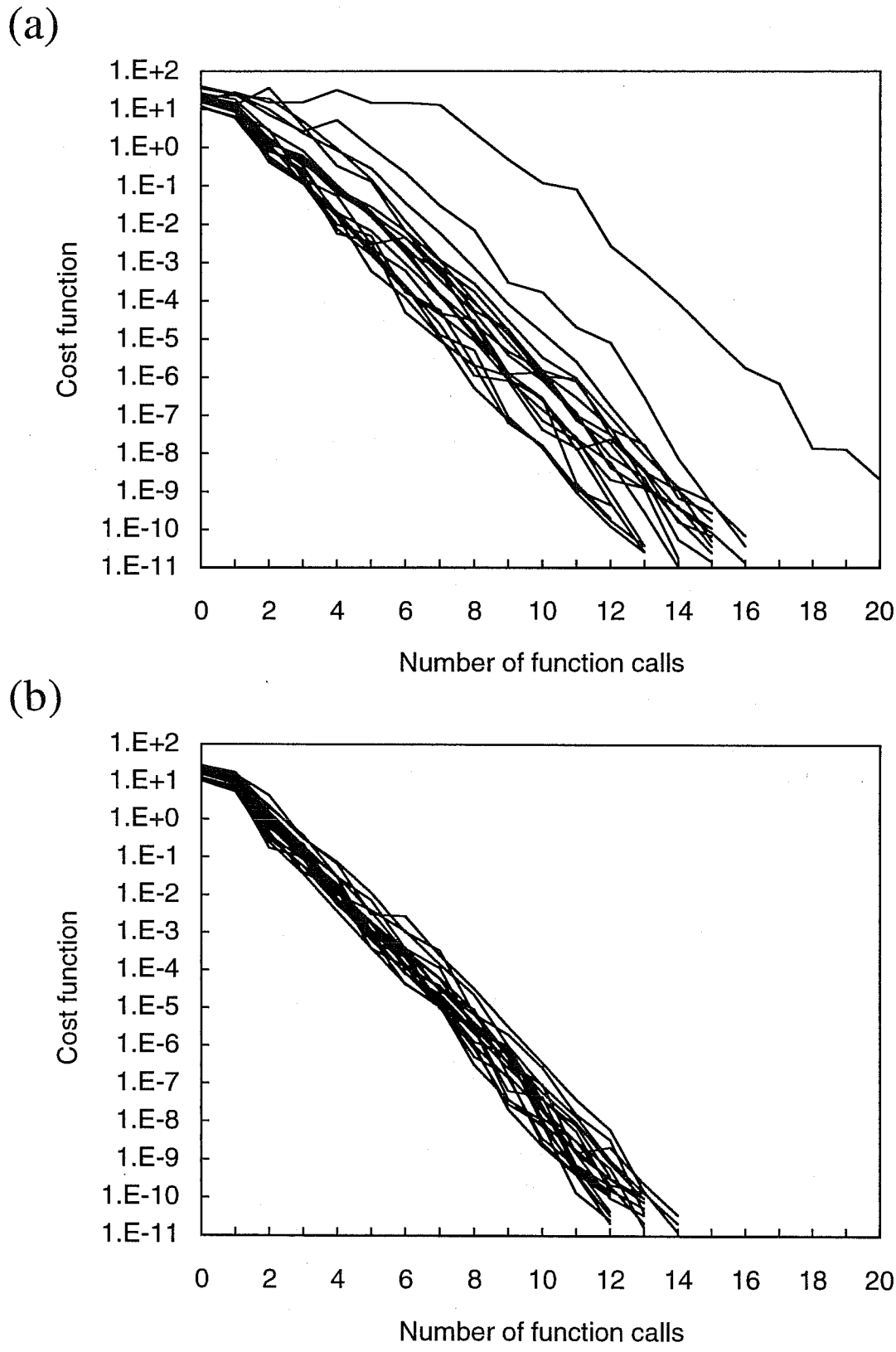

Fig.1 Variations of the cost function with the number of function calls for the column model assimilation experiment using (a) the original version and (b) the smoothed version of the moist processes. Each experiment consists of 20 cases using different initial guesses. Accurate observations of the model state variables are available at the beginning and end of a 6-hour assimilation windows. The ordinate is on a logarithmic scale.

r denotes the penalty parameter, $\frac{\partial D}{\partial t}$ the time tendency of model divergence at all time levels, and $\mathbf{W}$ a positive-definite symmetric matrix consisting of weights to calculate the global mean. The model state variables at all time levels are determined by the initial condition $\boldsymbol{x}_0$ for the assimilation window, and, therefore, the cost function is function of $\boldsymbol{x}_0$. The control variables are defined in the physical space in the first experiment. The L-BFGS method (Liu and Nocedal, 1989) is used to minimize the cost function. The maximum number of iterations is set to 30. Simple scaling is applied to accelerate convergence.

An idealized observation network is used in which the observations are provided at model Gaussian grid points (approximately $2.8125\ ^\circ \times 2.8125\ ^\circ$) and model vertical levels. The observation network is sparse in the tropics and the Southern Hemisphere. North of 30 °N observations of wind and temperature at all model levels, relative humidity at the lowest 10 levels, and surface pressure are available at the beginning and end of the assimilation window. These observations are intended to correspond to radiosonde observations in the real observation network. South of 30 °N wind observations are available only at $\sigma = 0.2$ and $\sigma = 0.85$, corresponding to cloud drift winds measured by geostationary satellites. Temperature observations at all model levels and surface pressure observations are available as in the north of 30 °N region. The former observations are intended to correspond to vertical temperature soundings by polar-orbiting satellites; the latter to ship, buoy, and other surface observations. The above three observations are provided at the beginning and end of the assimilation window. Relative humidity observations are not available south of 30 °N. Instead, 1-hour accumulated precipitation data are available every hour. Observations are generated by adding random error to the truth. Observation errors are assumed to be homogeneous, independent of each other, and normally distributed with no bias. The standard deviations of observation error for wind, temperature, relative humidity, and surface pressure are set to 3 m s^{-1}, 1 K, 10 %, and 1 hPa, respectively. The standard deviation of observation error for 1-hour precipitation is taken as 0.5 mm for the area average over one Gaussian grid box. The precipitation error is added to the true precipitation only if the latter is positive. Negative values of observed relative humidity and 1-hour precipitation data are replaced by zeros. To cancel the horizontal inhomogeniety of the Gaussian grid distribution, the cost function is defined in terms of the area integral over the globe rather than the summation over the Gaussian grid points.

Three assimilation methods are compared. The first method, hereafter referred to as NOMP, uses the assimilation model and the adjoint model without the moist processes. Since the moist processes are not included, supersaturation of water vapor is not removed during the forward integration. Yet, since the final analysis is prepared using the full-physics model, the NOMP method is capable of yielding analysis of precipitation and other related fields. The second method, hereafter referred to as MP, uses the models with the moist processes included but does not assimilate precipitation observations. The third method, hereafter referred to as MP+RR, uses the same models as MP but assimilates precipitation data. Comparison of the three methods will reveal the importance of moist processes for 4D-VAR in the tropics and the benefits of assimilating precipitation data.

3.2 **Verification of gradient calculation**

Prior to discussing results of the experiments, the correctness of the gradient calculation using the adjoint

method is verified. If the cost function has continuous partial derivatives of order two in the neighborhood of $\boldsymbol{x}_0$, application of the Taylor's theorem to the cost function yields

$$\varphi(\alpha) = \frac{J(\boldsymbol{x}_0) - J(\boldsymbol{x}_0 - \alpha \mathbf{S}^2 \nabla_{x_0} J)}{\alpha (\nabla_{x_0} J)^{\mathrm{T}} \mathbf{S}^2 \nabla_{x_0} J} = 1 + O(\alpha), \tag{4}$$

where α is a small nondimensional parameter and $\mathbf{S}$ is a scaling matrix for the gradient of the cost function. For sufficiently small α but not too close to the machine accuracy, the value of $\varphi(\alpha)$ should be close to unity if the gradient $\nabla_{x_0} J$ is correctly calculated.

The variation of $\varphi(\alpha)$ with log α for NOMP and MP are plotted in Fig.2. In this example $\boldsymbol{x}_0$ is taken as the truth at t = -48 h. The observations for the north of 30 °N region are assumed to be available over the globe. The observation errors are not added, nor is the penalty term included. Although it may be better to verify that $\varphi(\alpha) - 1$ is of order α, this is not easy for 4D-VAR with the moist processes included due to the fact that tangent linear approximation is less valid in this case. It is seen from Fig.2 that the value of $\varphi(\alpha)$ for NOMP is almost equal to unity for α less than 10^{-3}, while for MP $\varphi(\alpha)$ is close to one for α less than 10^{-5}. Larger values of $\varphi(\alpha)$ for α less than 10^{-10} result from numerical cancellation error, so they are to be neglected. Since the gradients of the cost function for the two cases are not very different (e.g., $|\mathbf{S} \nabla_{x_0} J|$ = 293.0 for NOMP, 278.9 for MP, and the cosine of angle between the two gradient vectors is 0.958), the difference in $\varphi(\alpha)$ may primarily reflect the difference in the shape of the cost function. The existence of a local minimum around $\alpha = 10^{-4}$ for MP indicates that the cost function in the direction of the scaled gradient is not convex. Given the highly nonlinear character of physical parameterizations, a cost function including moist processes has a more complicated shape with, possibly, multiple minima. These factors render the minimization for 4D-VAR with moist processes more difficult than for 4D-VAR without moist processes.

3.3 **Convergence performance**

Figure 3 shows the variation of the cost function as a function of the number of iterations in the minimization process for the three assimilation methods. Convergence performance is evaluated for two values of the penalty parameter r. The upper panel is for $r = 4 \times 10^{17}$ s^4; the lower panel is for $r = 1 \times 10^{18}$ s^4. In each panel the upper three lines are the discrepancy terms for observations except for precipitation, J_{OBS}, the middle three lines are the penalty terms, J_{PNL}, and the lower line is the discrepancy term for precipitation, J_{RR}, for MP+RR.

For $r = 4 \times 10^{17}$ s^4 the inclusion of the moist processes considerably slows down the convergence (Fig.3a). In particular, the MP method requires up to 49 function calls for 30 iterations and, still, the value of J_{OBS} after 30 iterations is much larger than that for NOMP. Step-like variations in J_{OBS} for MP and MP+RR results from the occasional occurrence of very small step lengths in the line search. Such instances are often associated with large gradients in the cost function. Comparison of MP and MP+RR reveals that assimilating precipitation data accelerates the convergence of 4D-VAR with the moist processes included. However, this is not always the case when real precipitation data are assimilated. In the simulated data framework observed precipitation data are fairly consistent with the model. Thus, the acceleration of convergence by

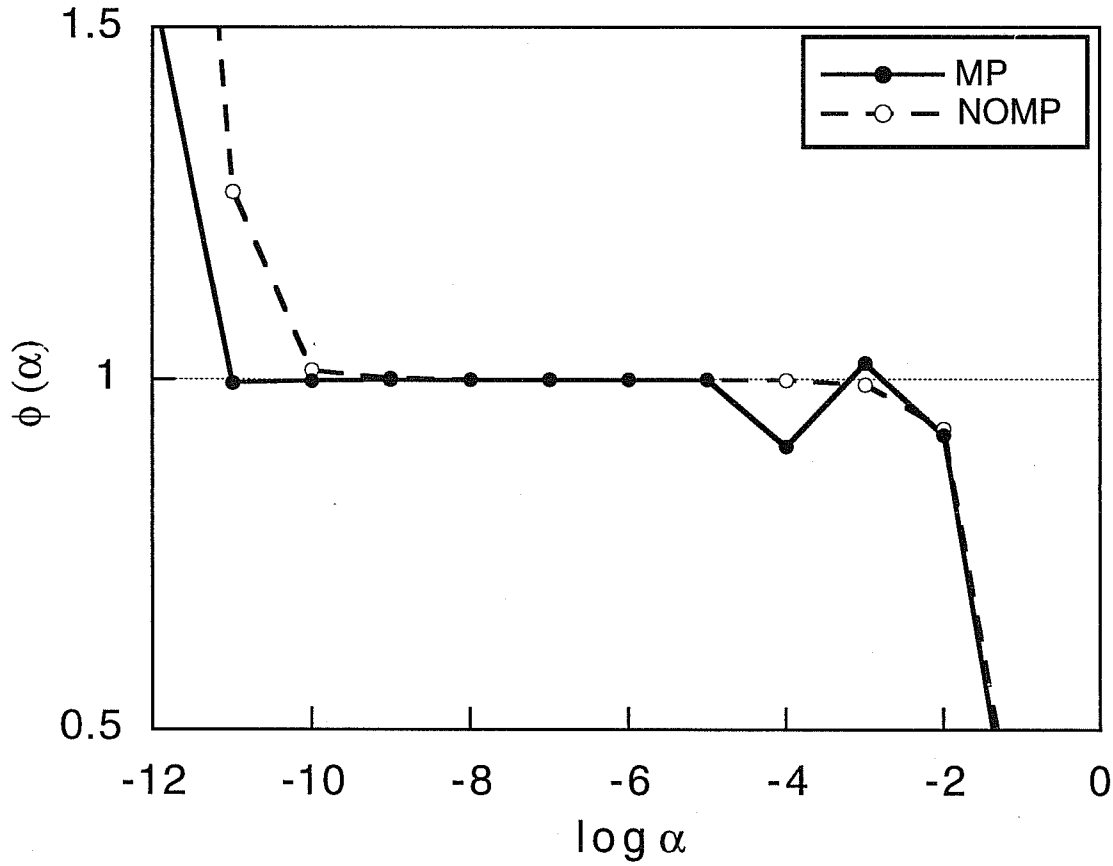

Fig.2 Variations of the function $\varphi(\alpha)$ with $\log \alpha$ for NOMP and MP. The truth at t = -48 h is taken as x_0. The observation errors and the penalty term are not included.

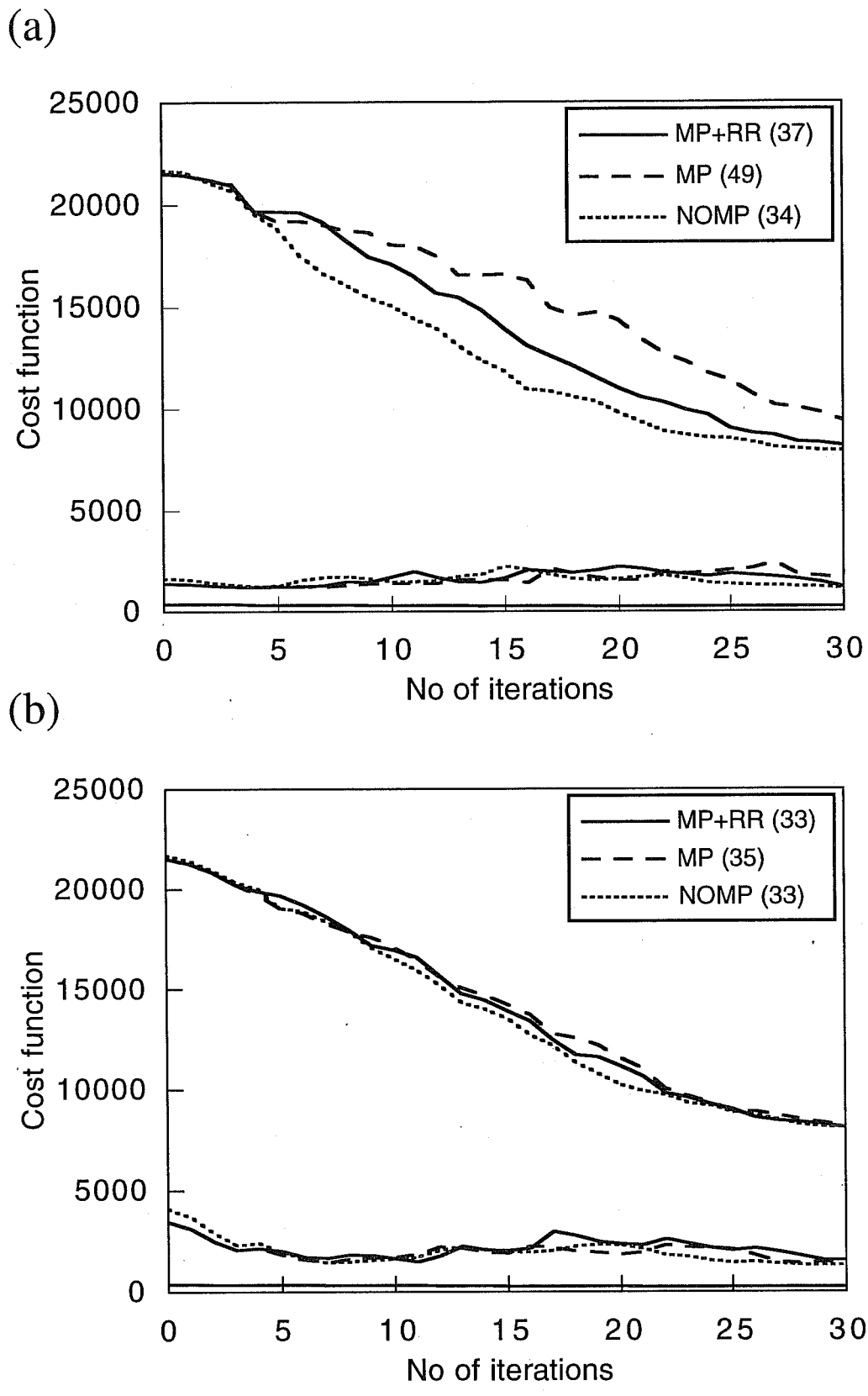

Fig.3 Variations of the cost function with the number of iterations for NOMP, MP, and MP+RR with (a) $r = 4 \times 10^{17}$ s^4 and (b) $r = 1 \times 10^{18}$ s^4. In each panel, the upper three lines are the discrepancy terms for conventional data, the middle three lines are the penalty terms, and the lower line is the discrepancy terms for precipitation data for MP+RR. Parenthetical values in the legend indicate the number of function calls required for 30 iterations.

assimilating precipitation data may be an expected result. The value of J_{PNL} after 30 iterations is almost the same as the value before the iteration (iteration 0) for the three methods, with a slight increase after around 10 iterations. J_{RR} is only a small fraction of the total cost function.

The convergence for MP and MP+RR is accelerated by using the larger penalty parameter, $r = 1 \times 10^{18}$ s^4 (Fig.3b). In particular, the number of function calls for MP is greatly reduced from 49 to 35. The number of function calls for MP+RR is still less than that for MP, indicating again the benefit of assimilating precipitation data. On the other hand, the convergence performance of NOMP is slightly deteriorated, although it is still better than that of MP and MP+RR. The excessive suppression of gravity wave level makes it difficult to fit the model solution to the observations and, therefore, decelerates the convergence (Courtier and Talagrand, 1990; Thépaut and Courtier, 1991). The values of J_{PNL} decrease during the first several iterations for the three methods and increase after around 10 iterations.

Results shown in Fig.3 suggest that the an appropriate control of gravity wave level increases the efficiency of 4D-VAR with the moist processes included. The moist processes tend to generate a large time tendency of divergence and also tend to introduce locally large gradients in the cost function. Therefore, it may be expected that encountering locally large gradients can be avoided, at least in the early stages of the minimization, by including a penalty term which suppresses a large time tendency of divergence. The sensitivity of the convergence rate on the penalty parameter is further investigated in the second experiment.

3.4 **Analyzed fields**

Figures 4-6 compare the analyzed 6-hour accumulated precipitation, 200 hPa divergence, and mean sea level pressure, respectively, at $t = 0$ h after 30 iterations for $r = 1 \times 10^{18}$ s^4. The top panel in each figure shows the truth, as defined from the full-physics simulation. A developing tropical cyclone east of the Philippines (Fig.6a) brings heavy precipitation (Fig.4a) and an accompanying pattern of strong divergence at 200 hPa (Fig.5a). This simulated cyclone corresponds to Super Typhoon Hope (27 July-3 August 1979) in the real atmosphere, so that it is referred to as a typhoon hereafter. Another tropical disturbance with heavy precipitation and strong divergence is found in the northern Arabian Sea. 4D-VAR without the moist processes considerably underestimates precipitation in the tropics and almost completely fails to retrieve the areas of heavier precipitation (Fig.4b). The strong divergence associated with the typhoon and the other tropical disturbance is also considerably underestimated as well as strong divergence in the eastern tropical Atlantic (Fig.5b). The sharp structure of the typhoon seen on the mean sea level pressure map is not well reproduced (Fig.6b).

Inclusion of the moist processes greatly improves the analysis of 6-hour accumulated precipitation (Fig.4c). Regions of heavy precipitation are well retrieved, although they are still underestimated in several areas and the locations of maximum precipitation east of the Philippines and in the Bay of Bengal are misplaced. The analysis of strong divergence in the northern Arabian Sea and eastern tropical Atlantic is improved (Fig.5c). The retrieved divergence in the region from the Bay of Bengal to the western tropical Pacific is still not satisfactory. The center of the divergence associated with the typhoon is erroneously shifted eastward,

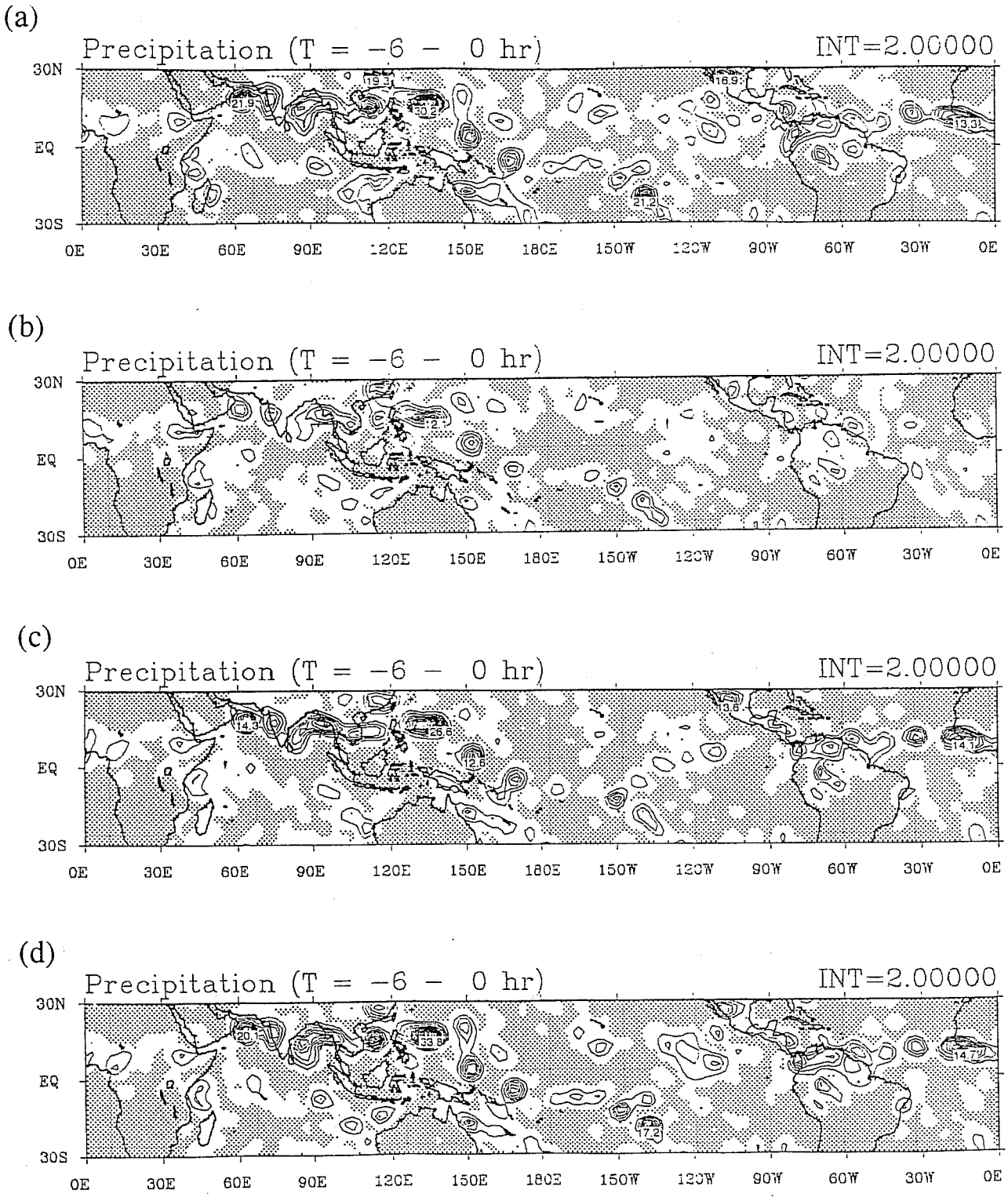

Fig.4 6-hour accumulated precipitation over the assimilation window for (a) the truth, (b) NOMP, (c) MP and (d) MP+RR with $r = 1 \times 10^{18}$ s^4. Contour interval is 2 mm. Areas less than 0.2 mm are shaded.

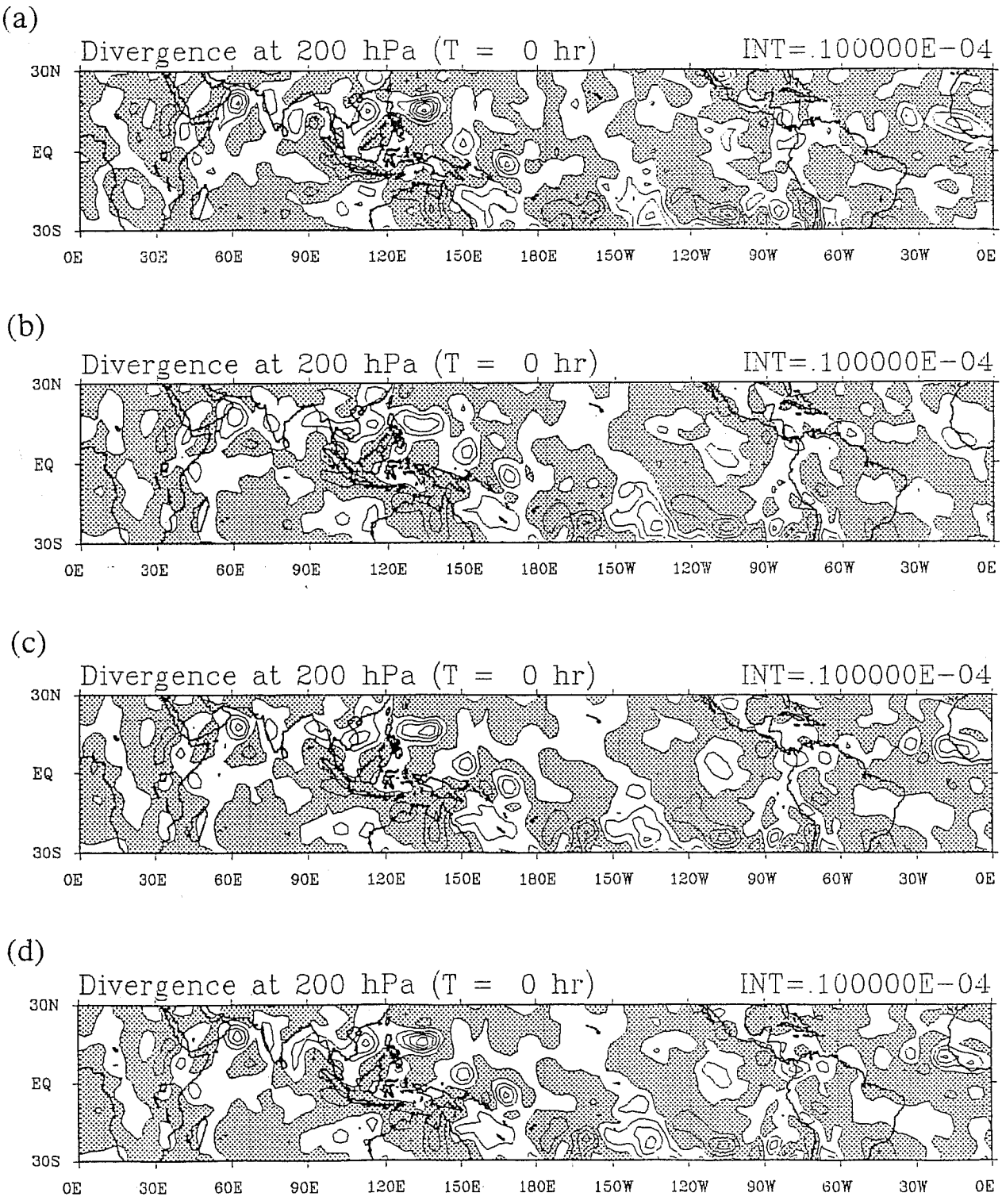

Fig.5 Divergence at 200 hPa at the end of assimilation window for (a) the truth, (b) NOMP, (c) MP and (d) MP+RR with $r = 1 \times 10^{18}$ s^4. Contour interval is 1×10^{-5} s^{-1}. Negative areas are shaded.

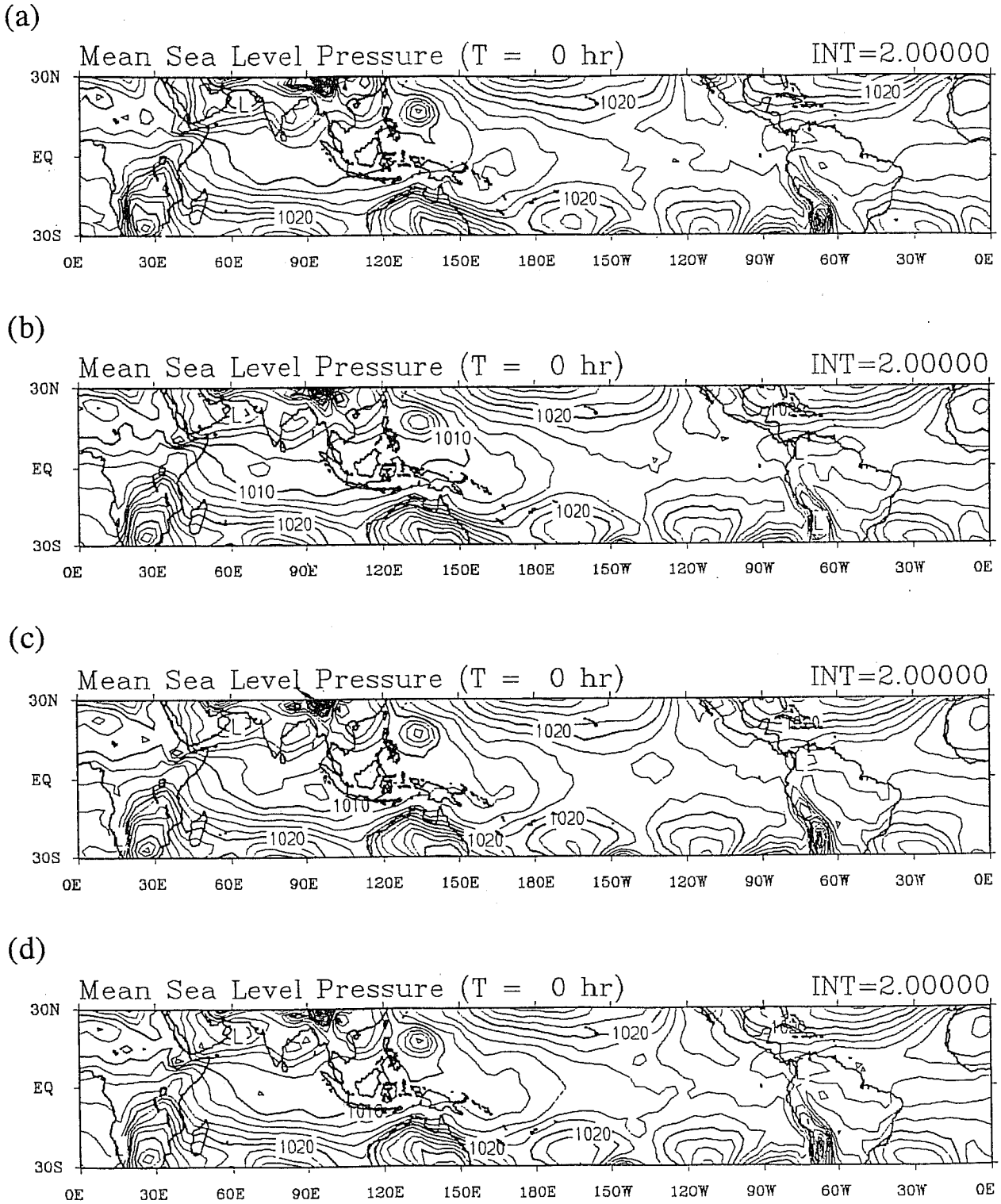

Fig.6 Mean sea level pressure at t= 0 h for (a) the truth, (b) NOMP, (c) MP and (d) MP+RR with $r = 1 \times 10^{18}$ s^4. Contour interval is 2 hPa.

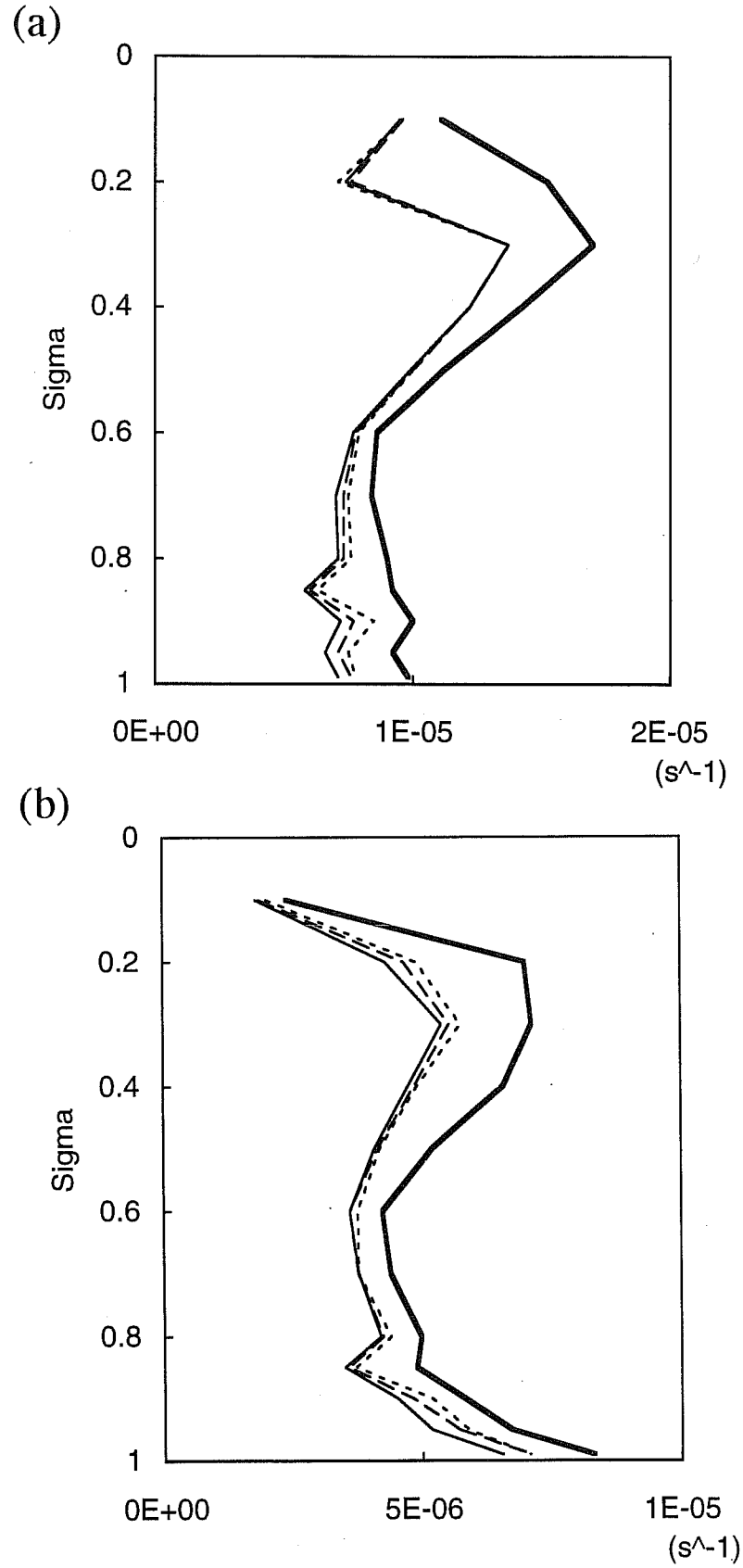

Fig.7 Vertical distribution of the root mean square error in (a) vorticity, (b) divergence, (c) temperature, and (d) relative humidity in the tropics (30 °N-30 °S) at the end of assimilation window with $r = 1 \times 10^{18}$ s^4. Thick solid line is the initial guess, dotted line is NOMP, dashed line is MP, and thin solid line is MP+RR.

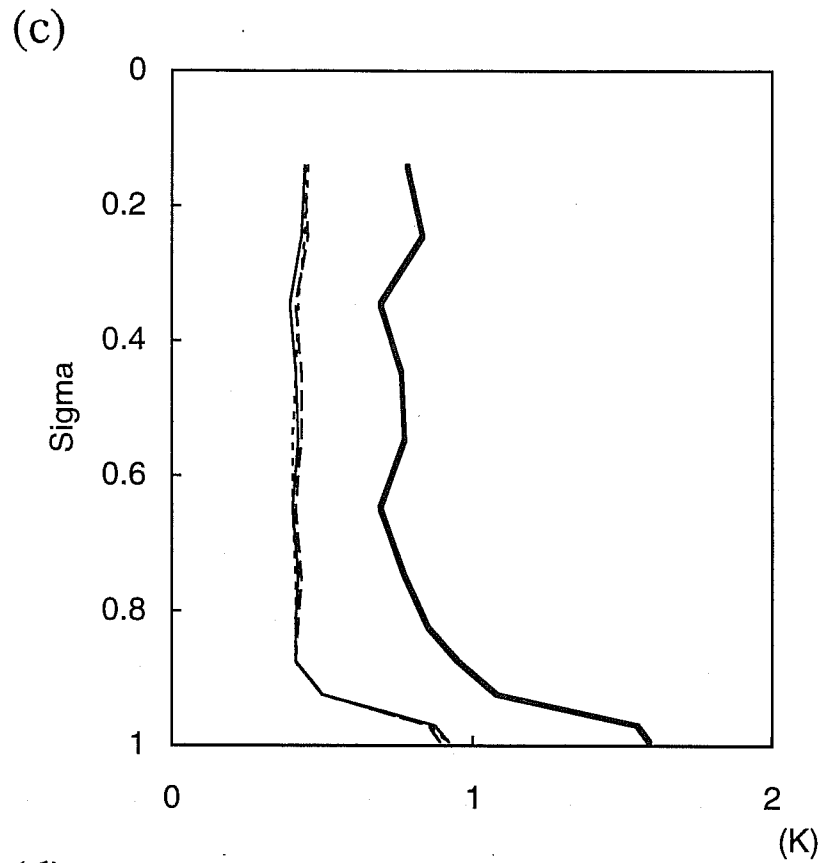

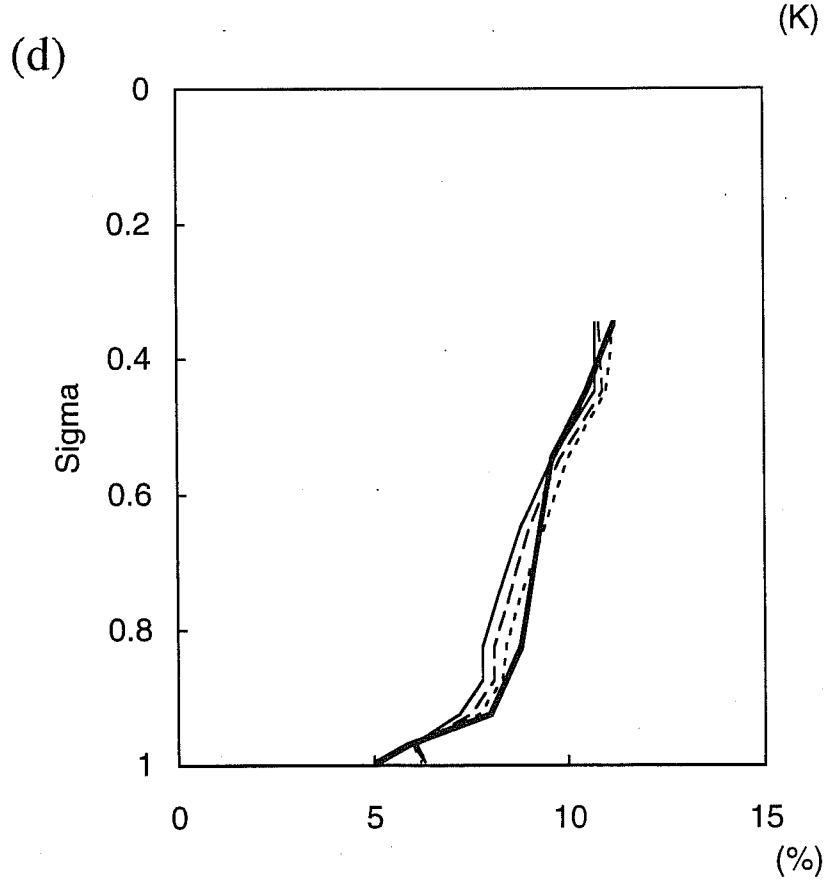

Fig.7 Continued

corresponding to the misplaced maximum of 6-hour accumulated precipitation. The central pressure of the simulated typhoon is slightly underestimated (Fig.6c). Assimilation of precipitation data with 4D-VAR works very well. Taking into account the observation error in precipitation data, agreement between the analyzed precipitation and the truth is remarkable (Fig.4d). The divergence field in the region from the Bay of Bengal to the western tropical Pacific is well retrieved (Fig.5d), although the divergence associated with the typhoon is slightly underestimated. The central pressure of the retrieved typhoon is almost the same as the truth (Fig.6d).

The vertical distributions of analysis error in vorticity, divergence, temperature and relative humidity in the tropics at $t = 0$ h are displayed in Fig.7. Because wind observations are available at $\sigma = 0.20$ and $\sigma = 0.85$ in the tropics, analysis errors in vorticity and divergence at these two levels are considerably decreased from the initial guess errors. Analysis errors at other levels in these fields are also decreased from the corresponding initial guess errors without using specific analysis structure functions. This is a nice property of 4D-VAR. A similar advantage of 4D-VAR is seen in the relative humidity analysis error. Relative humudity errors in the lower troposphere for MP and MP+RR are smaller than the initial guess error despite the fact that no moisture observations are available in the tropics. Positive impacts from including the moist processes and assimilating precipitation data are evident in the analyses of divergence, moisture, and lower tropospheric vorticity. In particular, the winds in the tropical planetary boundary layer are better analyzed. This result may reflect the fact that circulation in the tropical planetary boundary layer is closely related to cumulus convection. The impacts, however, are not clear for the temperature analysis. This is partly because temperature observations with relatively small errors are assumed to be available at all model levels and, as a result, the impact of model dynamics and the other observations on the temperature analysis is negligible.

4. ASSIMILATION EXPERIMENT USING REAL DATA

4.1 **Experimental design**

The 12-hour period 0-12 UTC 22 August 1992 is chosen as the assimilation window. Assimilated data are radiosonde and pibal data over the globe and SSM/I precipitation rates over the tropical oceans. The National Centers for Environmental Prediction (NCEP) operational analysis at the beginning of the assimilation window is initialized by using nonlinear normal mode initialization with physics. This initialized analysis serves as the initial guess for the model state at the same point. Different from the first experiment, the full-physics model is used as the assimilation model. Such a procedure has already been adopted by M. Zupanski (1993) and Zupanski and Mesinger (1995). The full-physics model may be more appropriate as the assimilation model when assimilating real observations even if the adjoint model uses the reduced physics. In this case, however, the adjoint model with the reduced-physics does not produce exact gradients of the cost function. The cost function is the same as in the first experiment. The control variables are defined in the spectral space, and the L-BFGS method is used for the minimization. The maximum numbers of iterations and function calls are set to 30 and 40, respectively. Three assimilation methods are compared as in the previous experiment. The NOMP method uses the adjoint model without the moist processes. The MP method uses the adjoint model with the moist processes included but does not assimilate the SSM/I precipitation rates. The MP+RR method uses the same adjoint model as in MP but assimilates the SSM/I precipitation rates.

Radiosonde and pibal data for 0-12 UTC 22 August 1992 are taken from the NCEP upper air data subsets archived at the National Center for Atmospheric Research (NCAR). Assimilated data are geopotential height at 1000 hPa, wind and temperature at 10 standard levels below 100 hPa and relative humidity at 6 standard levels below 300 hPa. Geopotential height data at the other levels are not assimilated because they are not independent of temperature, moisture, and 1000 hPa geopotential height data. Since the model top is placed at $\sigma = 0.1$, upper air data above 100 hPa are not assimilated. The observation error standard deviations used in this experiment are almost the same as those used in the NCEP operational 3D-VAR system (Parrish and Derber, 1992). Observation errors in the radiosonde and pibal data are assumed to be independent of each other, so that the observation error covariance matrix for these data is diagonal. The observation operators for the data consist of inverse spectral transforms to go from spectral to grid-point representation, conversions from model state variables to observed variables, bicubic horizontal interpolation from model Gaussian grid points to observation points, and cubic vertical interpolations from model sigma levels to observation levels. A simple quality control procedure is applied to the radiosonde and pibal data by using the NCEP operational analysis as a reference.

SSM/I brightness temperature data are provided by two polar-orbiting satellites, F10 and F11, in the Defence Meteorological Satellite Program (DMSP). The SSM/I precipitation rates over the tropical oceans are obtained from the regression formula developed by Olson et al. (1990). The bias and the root mean square error of the precipitation rate estimate are 0.13 mm h^{-1} and 0.59 mm h^{-1}, respectively. The SSM/I precipitation rates are gridded to a $1^\circ \times 1^\circ$ mesh over ocean between 35°N and 35°S by taking an area average. The 12-hour assimilation window is divided into 12 one-hour intervals. The SSM/I estimates of instantaneous precipitation rates belonging to one of the intervals are regarded as hourly mean precipitation rates over this one-hour interval. Bicubic interpolation is applied to interpolate model precipitation rates from model grid points to observation points. In view of the fact that model precipitation rates are computed in physical space not spectral space, bilinear interpolation might appear more appropriate. Results from an assimilation experiment using bilinear interpolation described in the next subsection suggest otherwise. A quality control procedure is not applied, nor is the bias in the Olson algorithm corrected. The observation error standard deviation of the SSM/I precipitation rates prepared on the $1^\circ \times 1^\circ$ grid is set to 1 mm h^{-1} as a crude estimate. Observation errors in the SSM/I precipitation rates are assumed to be horizontally uncorrelated. Since the radiosonde and pibal data and the SSM/I precipitation rates are independent of each other, the entire observation error correlation matrix is also diagonal.

Figure 8a shows the composite of the SSM/I precipitation rates over the assimilation window. It is seen that the SSM/I observations do not fully cover the tropical oceans: about a third of the tropical oceans remain unobserved. In this period there are no strong tropical disturbances except for Hurricane Andrew in the western Atlantic. A small region of precipitation at 25°N, 70°W adjacent to a data void region is related to this compact tropical cyclone. Unfortunately the center of the hurricane is not observed by the DMSP satellites during the assimilation window. However, even if the SSM/I observations covered the entire region, the horizontal scale of Hurricane Andrew is too small to be properly resolved by the T42L12 global spectral model. A region of heavy precipitation around 5°N, 165°E is associated with a tropical depression

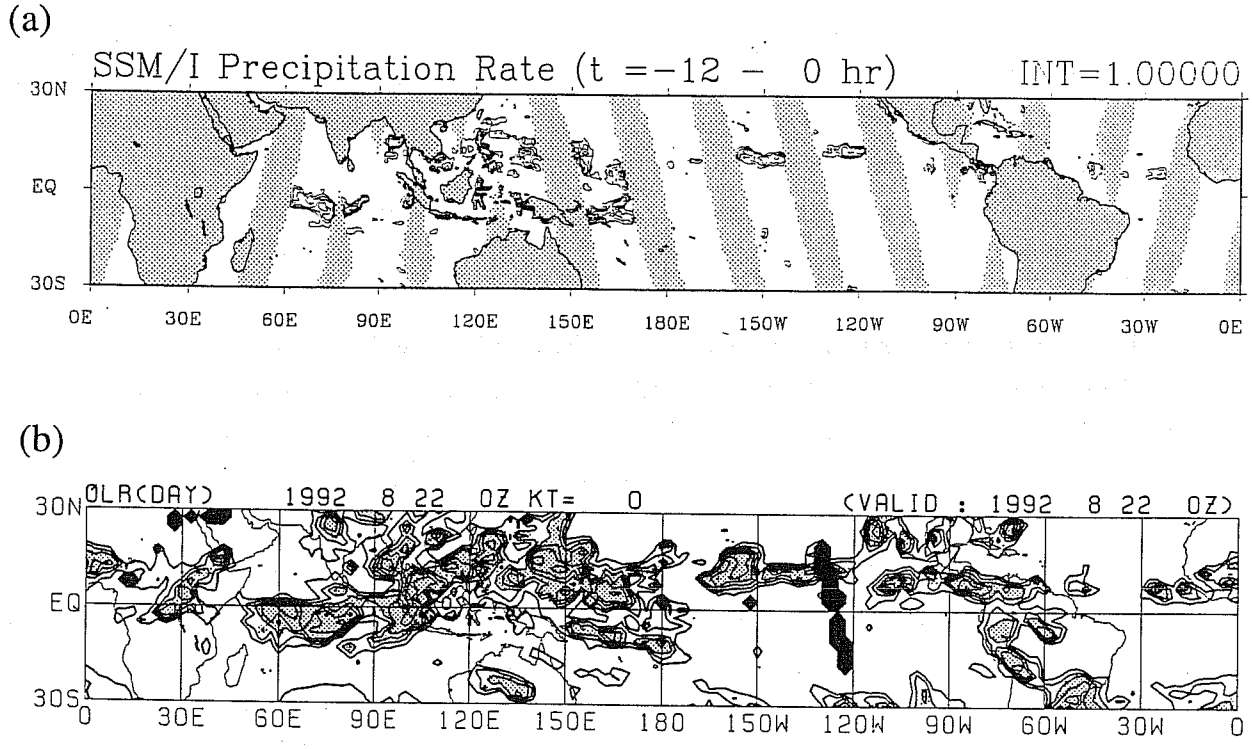

Fig.8 (a) Composite of SSM/I precipitation rates for 0-12 UTC 22 August 1992. Contour intervals are 0.25, 0.5, 1, 2, and 4 mm/h. Data void areas are shaded. (b) Composite of outgoing longwave radiation measured by NOAA satellites for day pass for 22 August 1992. Contour interval is 25 W m^{-2} and contours greater than 250 W m^{-2} are omitted. Areas of less than 200 W m^{-2} are lightly shaded. Data void areas are densely shaded.

that is developing into Super Typhoon Omar.

Outgoing longwave radiation (OLR) data obtained from the infrared radiometer aboard polar-orbiting NOAA satellites have more data coverage in the tropics. Although OLR data have a poorer physical basis for estimating precipitation rates, low OLR values generally correspond to heavy precipitation. Figure 8b displays the day pass composite of OLR for 22 August 1992. Since OLR data used for this composite between 110°E and 180°E fall into the assimilation window of 0-12 UTC 22 August 1992, the OLR composite in this region can be compared with the SSM/I composite. General agreement between the two composites in the region suggests that the OLR composite can be used to qualitatively verify the precipitation analysis by 4D-VAR in SSM/I data void regions.

4.2 **Convergence performance**

The cost functions computed by the adjoint models are plotted in Fig.9 as a function of the number of iterations for NOMP, MP, and MP+RR. The NOMP method shows better convergence performance than the MP and MP+RR methods as in the first experiment. If the cost function has locally large gradients resulting from the highly nonlinear nature of physical processes, a better approximation to the gradient of the cost function does not always leads to better convergence performance. It is seen that the assimilation of the SSM/I precipitation rates also slightly degrade the convergence. This result is in contrast to results in the previous experiment where assimilation of precipitation data accelerated the convergence rate. The value of the penalty term remains almost constant during the minimization process for the three methods. Since the initial guess used is the initialized operational analysis, the gravity wave level at iteration 0 may already be at a reasonable level. Therefore, the almost constant penalty terms indicate that the resulting analyses after 30 iterations also have acceptable gravity wave levels.

Figure 10 shows the sensitivity of convergence performance to the penalty parameter r for MP+RR. The cost functions are plotted as a function of the number of iterations for the following three penalty parameters: $r = 5 \times 10^{20}$ s^4, 8×10^{20} s^4, and 15×10^{20} s^4. Minus signs in the parentheses in the legends indicate that the number of function calls reaches the maximum value, 40, before 30 iterations. It is seen that there is an optimal value of the penalty parameter, $r = 8 \times 10^{20}$ s^4, which gives the best convergence performance. It also keeps the magnitude of the penalty term almost constant. When $r = 5 \times 10^{20}$ s^4 is used, the convergence is considerably decelerated and the maximum number of function calls is reached before 28 iterations. This result agrees with results from the previous experiment: too small penalty parameters lead to a poor convergence performance of 4D-VAR with the moist processes included. The penalty term gradually increases during the minimization process, indicating that gravity wave level is too high towards the end of iteration. When $r = 15 \times 10^{20}$ s^4 is used, the convergence performance is also degraded. A decreasing tendency of the penalty term during the minimization process indicates that the gravity wave level is excessively suppressed.

So far, bicubic interpolation has been used to interpolate model precipitation rates from model grid points to observation points. In view of the fact that model precipitation is calculated in physical space not spectral space and that convective rainfall, which predominates in the tropics, is a rather localized phenomenon, bilinear interpolation might appear more appropriate. Figure 11 compares convergence performance between

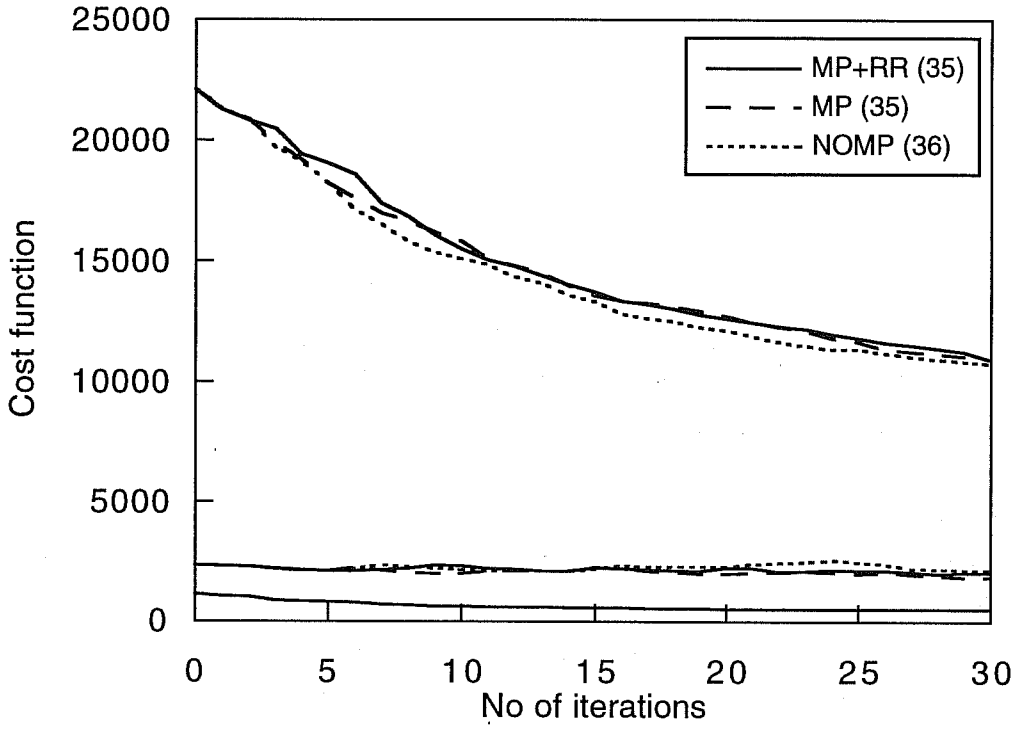

Fig.9 Variations of the cost function with the number of iterations for NOMP, MP, and MP+RR with $r = 8 \times 10^{20}$ s^4. The upper three lines are the discrepancy terms for radiosonde and pibal data, the middle three lines are the penalty terms, and the lower line is the discrepancy term for precipitation data for MP+RR. Parenthetical values in the legend of each panel indicate the number of function calls required for 30 iterations.

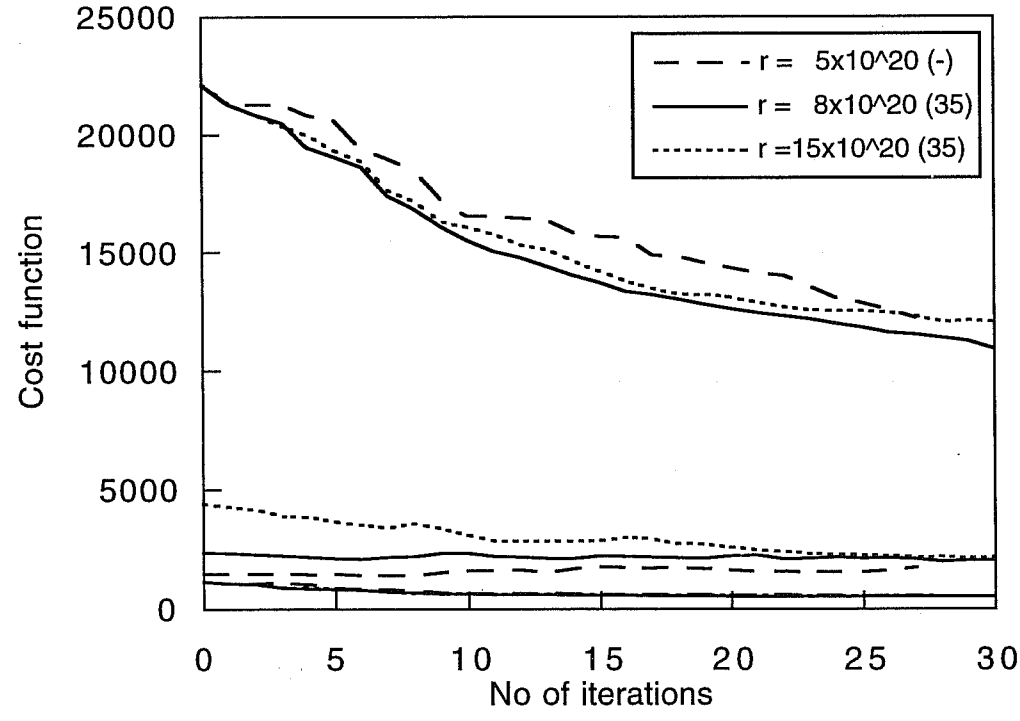

Fig.10 Same as Fig.9, except for MP+RR with $r = 5 \times 10^{20}$ s^4, 8×10^{20} s^4, and 15×10^{20} s^4. The upper three lines are the discrepancy terms for radiosonde and pibal data, the middle three lines are the penalty terms, and the lower three lines are the discrepancy terms for precipitation data.

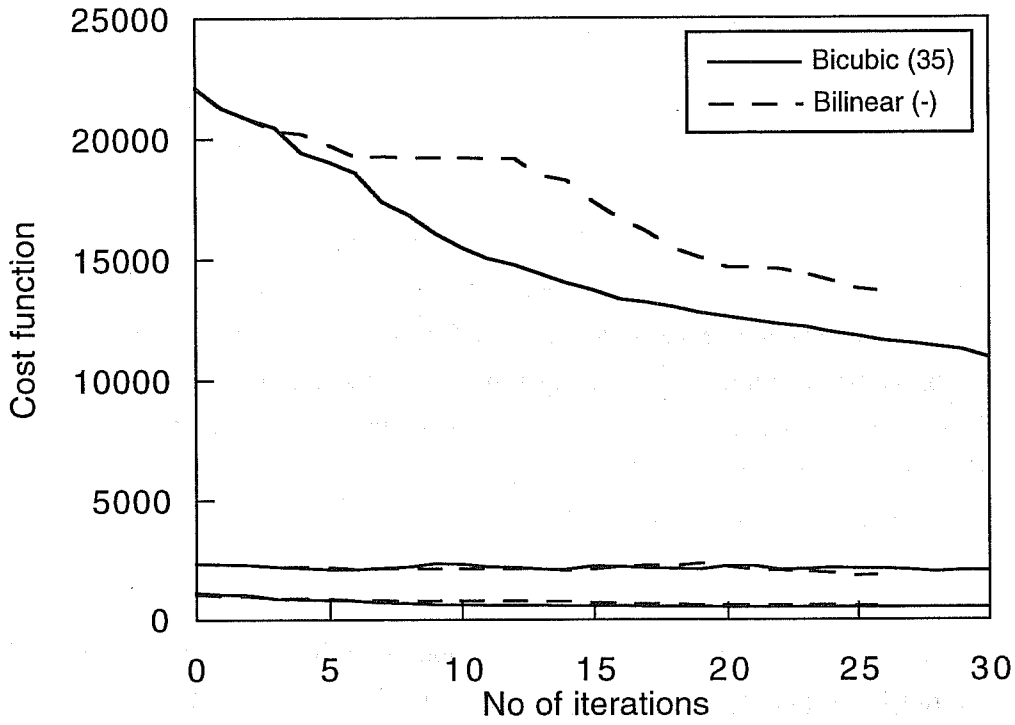

Fig.11 Same as Fig.9, except for MP+RR with the bicubic and bilinear interpolations for precipitation data. The upper two lines are the discrepancy terms for radiosonde and pibal data, the middle two lines are the penalty terms, and the lower two lines are the discrepancy terms for precipitation data.

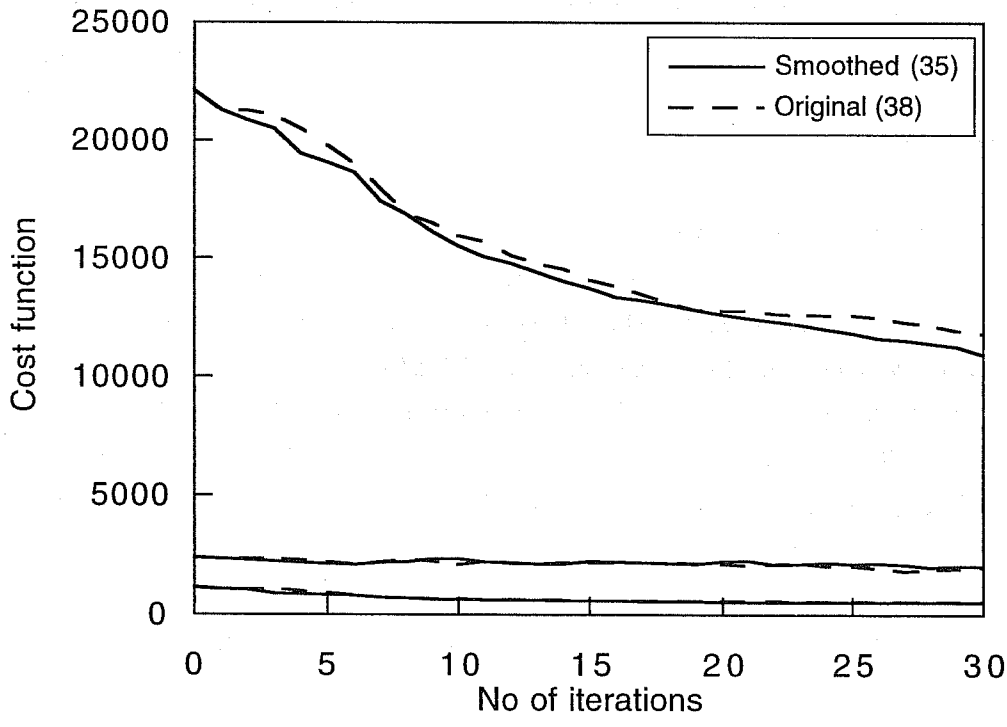

Fig.12 Same as Fig.9, except for MP+RR with the original and smoothed moist processes. The upper two lines are the discrepancy terms for radiosonde and pibal data, the middle two lines are the penalty terms, and the lower two lines are the discrepancy terms for precipitation data.

bicubic and bilinear interpolations for MP+RR. The penalty parameter r is set to 8×10^{20} s^4. It is seen that the convergence rate is considerably decelerated when bilinear interpolation is used; the maximum number of function calls are reached before 27 iterations. A higher-order interpolator has a further smoothing effect on the cost function and, as a result, may improve convergence performance.

The column model assimilation experiment described at the end of section 2 demonstrated that the original discontinuous moist processes lead to slower convergence rates. It is interesting to examine to what extent the smoothed moist processes improve the convergence performance when using the global primitive-equation model and real observations. An assimilation experiment is performed for MP+RR with $r = 8 \times 10^{20}$ s^4 using the original version of the moist processes. Figure 12 compares the convergence performance between the original moist processes and the smoothed moist processes. It is seen that the original moist processes degrade the convergence performance of 4D-VAR.

4.3 **Analyzed fields**

Figure 13 shows accumulated precipitation over the 12-hour assimilation window produced by the three methods. The corresponding accumulated precipitation obtained from the initial guess is also displayed for comparison. The initial guess precipitation is calculated by making a 12-hour prediction with the forward model from the initial guess. In order to evaluate the quality of these precipitation analyses we need observations of 12-hour accumulated precipitation over the tropics, but precipitation observations with sufficient spatial coverage and precision are not available. Here we assume that the spatial pattern of the true accumulated precipitation distribution is not very different from that of the composite of the SSM/I precipitation rates shown in Fig.8a. When using the SSM/I composite for verification purposes, only a qualitative comparison is possible. Since the SSM/I composite is not available over land and data void regions, the day pass composite of OLR shown in Fig.8b is also used as complementary data in the qualitative verification.

The spatial distribution of the initial guess precipitation (Fig.13a) exhibits several discrepancies with that of the SSM/I composite. For example, the initial guess generates heavy precipitation in the eastern Arabian Sea, but the SSM/I composite does not show large precipitation rates in this region. Regions of heavy precipitation over the equatorial Indian Ocean in the SSM/I composite are not seen in the initial guess precipitation. In the tropical Pacific a region of precipitation observed around 10°N, 135°E is misplaced southward by about 10°. A region of precipitation south of the Hawaii islands is missing in the initial guess precipitation. The spatial pattern of precipitation distribution produced by the NOMP method is almost the same as that of the initial guess precipitation, but precipitation amounts are different in several regions (Fig.13b). This result suggests that the adjoint model without moist processes is not adequate to retrieve precipitation in the tropics even if the full-physics model is used as the forward model.

When using the adjoint model with the moist processes included, significant changes in precipitation analysis are introduced in the western tropical Pacific (Fig.13c). The region of heavy precipitation north of New Guinea is shifted northward by about 10°, and the center of heavy precipitation just west of the date line is shifted westward by about 5°. A comparison with the SSM/I composite in Fig.8a reveals that the former

change makes the spatial pattern of analyzed accumulated precipitation closer to the SSM/I composite. The existence of a SSM/I data void region around the date line makes it difficult to find the center of the latter heavy precipitation region. The day pass composite of OLR in Fig.8b is useful for this purpose. As mentioned in subsection 4.1, the spatial pattern of the OLR composite in the western and central Pacific is expected to resemble that of the true accumulated precipitation over the assimilation window. The center of low OLR just west of the date line in the OLR composite is located at 5°N, 165°E. Thus, the position of the heavy precipitation produced by the MP method is closer to the observed position than that produced by the NOMP method. There are several radiosonde and pibal stations in the western tropical Pacific in contrast to the other tropical oceans. Observational data provided by these stations may contribute to the improved precipitation analysis in the western tropical Pacific. On the other hand, regions of heavy precipitation observed in the equatorial Indian Ocean and south of the Hawaii islands are not well retrieved by the MP method possibly because no radiosonde and pibal data are available in these areas. This result demonstrates the necessity of including the moist processes in the adjoint model for 4D-VAR in the tropics.

A comparison between Fig.8a and Fig.13d reveals that assimilation of the SSM/I precipitation rates with 4D-VAR works quite well. Regions of heavy precipitation in the equatorial Indian Ocean and south of the Hawaii islands are well retrieved. Erroneous areas of precipitation over the ocean around western India, northwest of Madagascar, and northwest of Australia are removed. The spatial distribution of precipitation produced by the MP+RR method in the western tropical Pacific exhibits a closer agreement with the OLR composite (Fig.8b) than that produced by the MP method even in SSM/I data void areas. Since wind speeds in the tropics are generally smaller than in the extratropics, significant horizontal advection of information from data available areas to data void areas is not expected when using a 12-hour assimilation window. The improvement in the precipitation analysis in SSM/I data void areas may primarily result from assimilating available observational data by using the model dynamics.

The time sequences of hourly mean precipitation rates at two Gaussian grid points at 7°N, 166°E and 4°S, 65°E are shown in Fig.14. These two points are near the centers of heavy precipitation regions in the precipitation analysis by the MP+RR method (Fig.13d). One-hour intervals in which the SSM/I precipitation rates are available are shaded in this figure. At the grid point in the western tropical Pacific (Fig.14a) the precipitation rates for the initial guess and NOMP are much smaller than those for MP and MP+RR. The precipitation rate produced by the MP+RR method is slightly larger than that produced by the MP method. In other words, the analyzed precipitation rates at this point are increased over the whole assimilation window by assimilating the SSM/I precipitation rates at the two one-hour intervals. At the grid point in the equatorial Indian Ocean the precipitation rates for the initial guess, NOMP, and MP are much smaller than that for MP+RR. The precipitation rate produced by the MP+RR method exhibits a decreasing tendency in the assimilation window. The SSM/I precipitation rates provided at the two one-hour intervals suggest a decreasing tendency of precipitation rates around this point, and that this observed time tendency is reflected in the analyzed MP+RR precipitation rates. A point to note here is that the impact of assimilating the SSM/I precipitation rates with 4D-VAR spreads over the whole assimilation window, not just simply around the observation times.

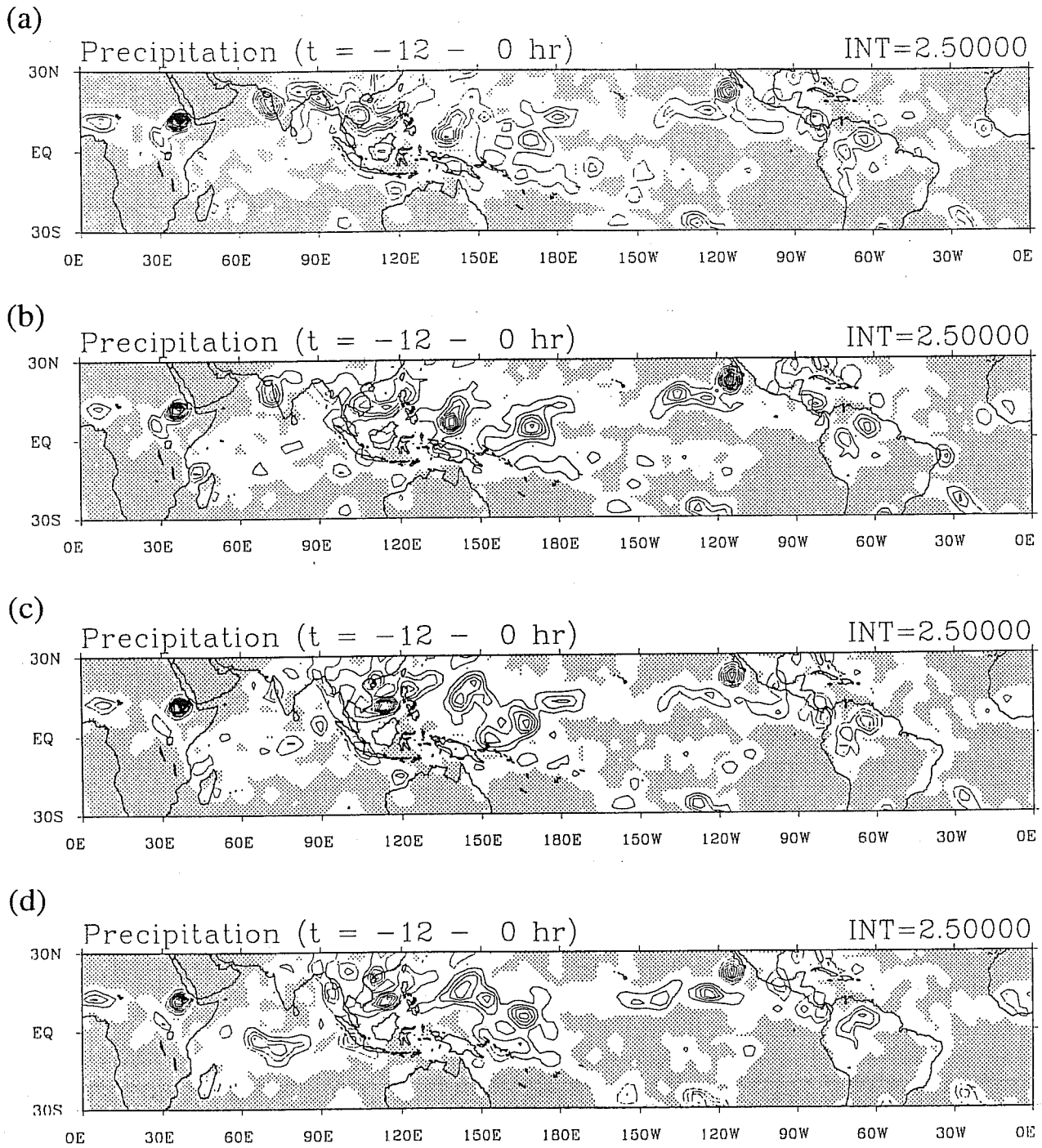

Fig.13 12-hour accumulated precipitation over the assimilation window for (a) the initial guess, (b) NOMP, (c) MP, and (d) MP+RR with $r = 8 \times 10^{20}$ s^4. Contour interval is 2.5 mm. Areas less than 0.25 mm are shaded.

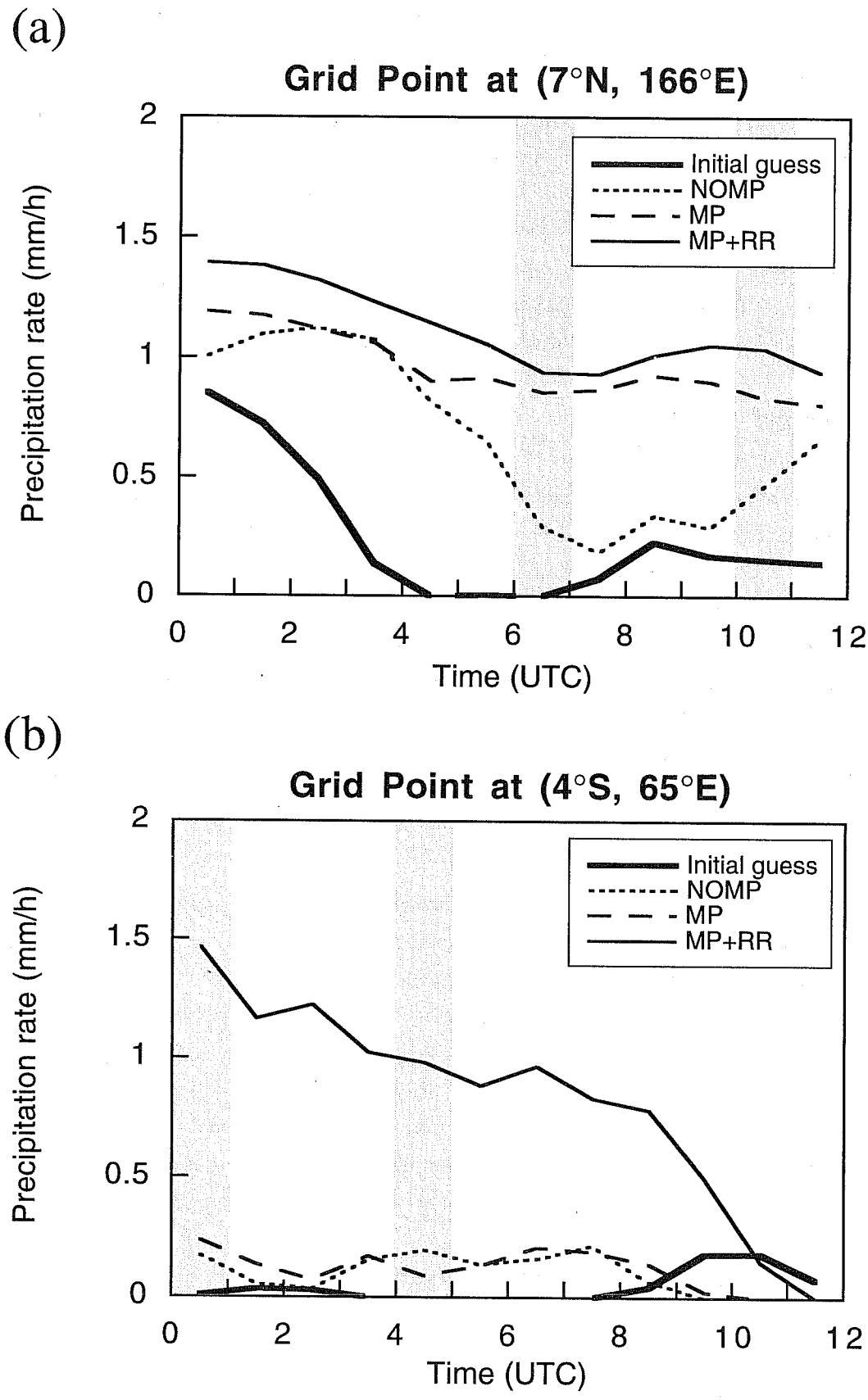

Fig.14 Time sequences of precipitation rates for the assimilation window at (a) 7°N, 166°E and (b) 4°S, 65°E. One-hour intervals when SSM/I observations are available are shaded.

Figure 15 compares analyzed 200 hPa divergence fields at the end of the assimilation window. Centers of strong divergence north of New Guinea obtained from the initial guess and the NOMP method are associated with the misplaced heavy precipitation in this region (see Figs.13a and b). Strong divergence west of India obtained from the initial guess is gradually replaced by convergence moving through the NOMP, MP, and MP+RR analyses. In similar fashion the upper level divergence associated with the developing tropical depression around 5°N, 165°E becomes stronger and more compact. A comparison between Figs.15c and d reveals that the impact of assimilating the SSM/I precipitation rates on divergence analysis is not very remarkable in this case. In the western Atlantic, possible strong divergence associated with Hurricane Andrew is not retrieved by any of the methods including the initial guess. This may be due to the fact that the spatial resolution of the model is not high enough to resolve this compact tropical cyclone.

5. CONCLUSIONS

The conclusions of this paper are as follows:

- 4D-VAR using the adjoint model which lacks the moist processes produces a poor analysis in the tropics even if the full-physics model is used as the forward model. Inclusion of the moist processes in the adjoint model yields a better analysis of precipitation, divergence, moisture, and lower-tropospheric vorticity. However, the convergence rate is decelerated by including the moist processes.
- The following three procedures improve the convergence performance of 4D-VAR using the adjoint model with the moist processes included: removal of discontinuities from parameterization schemes of the moist processes, appropriate control of gravity wave level, and use of a higher-order horizontal interpolation operator for precipitation when assimilating precipitation data.
- The impact of assimilating the SSM/I precipitation rates on the precipitation analysis is not confined to around SSM/I observation times, but spreads over the whole assimilation window.

Results from this study demonstrate the benefits of including moist processes in the adjoint model for 4D-VAR in the tropics. A problem introduced by the inclusion of moist processes is the degradation in the convergence performance due to less validity of the tangent linear approximation. Additional smoothing of the moist processes, especially parameterization schemes for deep cumulus convection, will improve the convergence performance. Introduction of preconditioning is also desirable for this purpose. A background term that was not considered in this study is capable of effectively controlling of gravity wave level in variational data assimilation. In light of the second conclusion of this study, it may be expected that inclusion of a background term in the cost function further improves the convergence performance. Another problem that was not addressed is the correction of model error. Since the largest part of forecast error in the tropics is due to model systematic error, introduction of a systematic error correction as proposed by Derber (1989) may be more important in the tropics than in the extratropics.

ACKNOWLEDGMENTS

This research was done during the author's visit to the Department of Meteorology of Florida State University. The author is sincerely thankful to Prof. T. N. Krishnamurti for providing the opportunity for the visit. The research was supported by NSF Grant ATM 9312537 and NASA Grants NAG 8-914 and NAG 5-1595. The computations for this work were carried out on the CRAY-C90 at San Diego Supercomputer Center and the

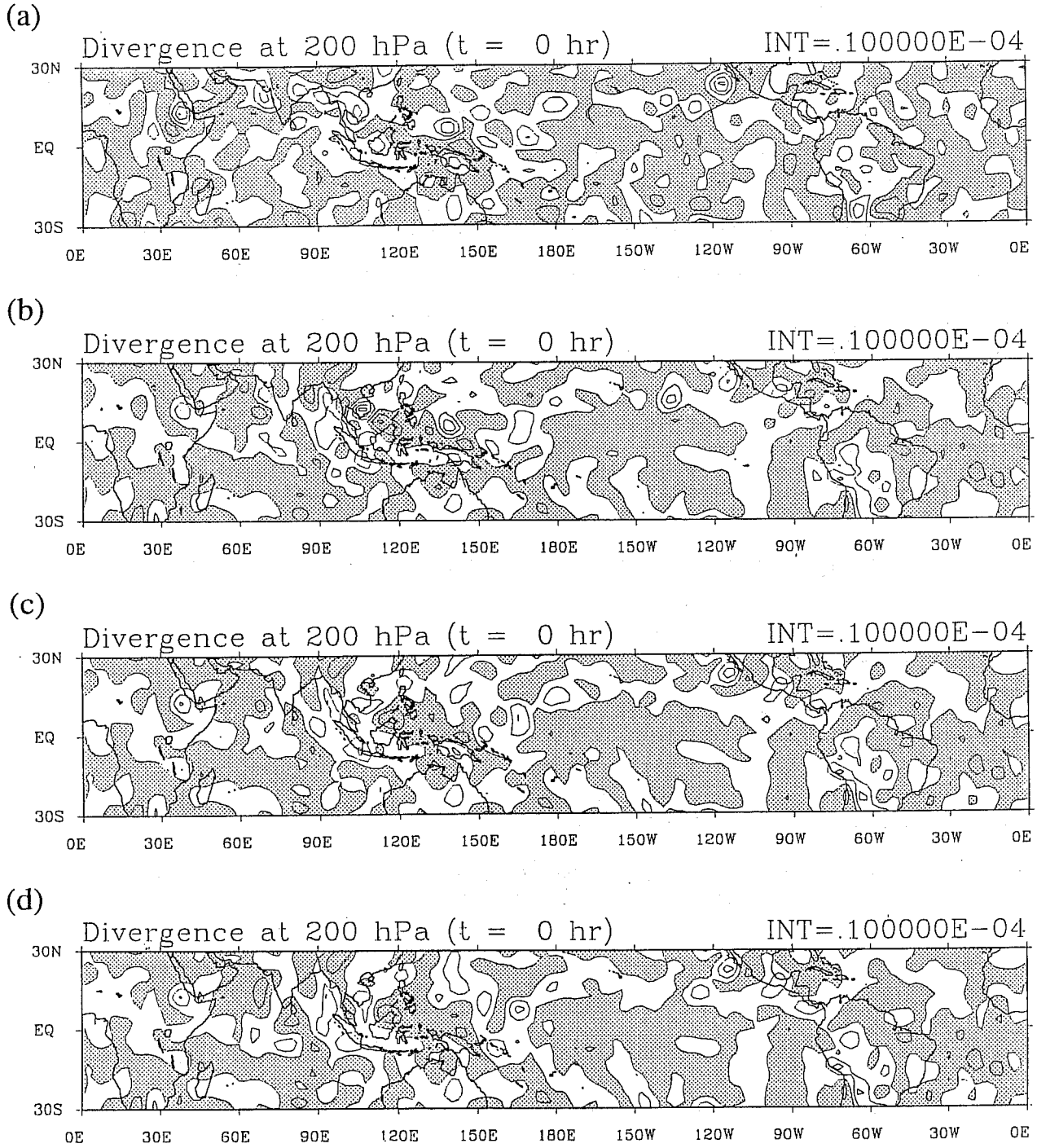

Fig.15 Divergence at 200 hPa at the end of assimilation window for (a) the initial guess, (b) NOMP, (c) MP and (d) MP+RR with $r = 8 \times 10^{20}$ s^4. Contour interval is 1×10^{-5} s^{-1}. Negative areas are shaded.

CRAY-YMP at Florida State University.

REFERENCES

Businger, J. A., J. C. Wyngard, Y. Izumi, and E. F. Bradley, 1971: Flux profile relationship in the atmospheric surface layer. J. *Atmos. Sci.*, **28**, 181-189.

Chang, C. B., 1979: *On the Influences of Solar Radiation and Diurnal Variation of Surface Temperatures on African Disturbances.* FSU Report No. 79-3, Department of Meteorology, Florida State University, 157pp.

Courtier, P., and O. Talagrand, 1990: Variational assimilation of meteorological observations with the direct and adjoint shallow-water equations. *Tellus*, **42A**, 531-549.

Derber, J. C., 1989: A variational continuous assimilation technique. *Mon. Wea. Rev.* **117**, 2437-2446.

Holton, J. R., 1992: *An Introduction to Dynamic Meteorology, Third Edition*. Academic Press, 511pp.

Krishnamurti, T. N., S. Low-Nam, and R. Pasch, 1983: Cumulus parameterization and rainfall rates II., *Mon. Wea. Rev.* **111**, 815-828.

Krishnamurti, T. N, K. Ingles, S. Cocke, R. Pasch, and T. Kitade, 1984: Details of low latitude medium-range numerical weather prediction using a global spectral model II. Effect of orography and physical initialization. *J. Meteor. Soc. Japan*, **62**, 613-649.

Liu, D. C., and J. Nocedal, 1989: On the limited memory BFGS method for large scale optimization, *Mathematical Programming*, **45**, 503-528.

Louis, J. F., 1979: A parametric model of vertical eddy fluxes in the atmosphere. *Bound.-Layer Meteor.*, **17**, 187-202.

Navon, I. M., X. Zou, J. C. Derber, and J. Sela, 1992: Variational data assimilation with an adiabatic version of the NMC spectral model. *Mon. Wea. Rev.*, **120**, 1433-1446.

Olson, W. S., F. J. LaFontaine, W. L. Smith, and T. H. Achtor, 1990: *Recommended algorithms for the retrieval of rainfall rates in the tropics using the SSM/I (DMSP-8)*. CIMSS/Space Science and Engineering Center, Univ. of Wisconsin, 10pp.

Parrish, D. F., and J. C. Derber, 1992: The National Meteorological Center's spectral statistical-interpolation analysis system. *Mon. Wea. Rev.*, **120**, 1747-1763.

Thépaut, J.-N., and P. Courtier, 1991: Four-dimensional variational data assimilation using the adjoint of a multilevel primitive-equation model. *Quart. J. Roy. Meteor. Soc.*, **117**, 1225-1254.

Thépaut, J.-N., D. Vasiljevic, P. Courtier, and J. Pailleux, 1993a: Variational assimilation of conventional meteorological observations with a multilevel primitive-equation model. *Quart. J. Roy. Meteor. Soc.*, **119**, 153-186.

Thépaut, J.-N., R. N. Hoffman, and P. Courtier, 1993b: Interactions of dynamics and observations in a four-dimensional variational assimilation. *Mon. Wea. Rev.*, **121**, 3393-3414.

Tsuyuki, T., 1996a: Variational data assimilation in the tropics using precipitation data. Part I: Column model. *Meteor. Atmos. Phys.* in press.

Tsuyuki, T., 1996b: Variational data assimilation in the tropics using precipitation data. Part II: 3D model. *Mon. Wea. Rev.* in press.

Tsuyuki, T., 1996c: Variational data assimilation in the tropics using precipitation data. Part II: Assimilation of SSM/I precipitation rates. *Mon. Wea. Rev.* submitted.

Zou, X., I. M. Navon, and J. Sela, 1993: Variational data assimilation with moist threshold processes using the NMC spectral model. *Tellus*, **45A**, 370-387.

Zupanski, D., 1993: The effects of discontinuities in the Betts-Miller cumulus convection scheme on four-dimensional variational data assimilation. *Tellus*, **45A**, 511-524.

Zupanski, D., and F. Mesinger, 1995: Four-dimensional variational assimilation of precipitation data. *Mon. Wea. Rev.*, **123**, 1112-1127.

Zupanski, M., 1993: Regional four-dimensional variational data assimilation in a quasi-operational forecasting environment. *Mon. Wea. Rev.*, **121**, 2396-2408.